Journal of Green Energy Research and Innovation

Optimal Configuration of Solar Combined Hydrogen, Heat, and Power (S-CHHP) by Considering Reliability Model

Mojtaba Pirmohammad Talatape, Sajad Bagheri, Reza Ghanizadeh, Mohammad Reza Miveh

Highlights

- **Presenting reliability model of solar-based-CHHP (S-CHHP).**
- **Utilizing LSTM-CNN to predict system uncertainties.**
- **Utilizing K-means clustering as a scenario reduction method.**
- **Combined hydrogen, heat and power (CHHP) to generate three kinds of energy demands.**

Graphical Abstract

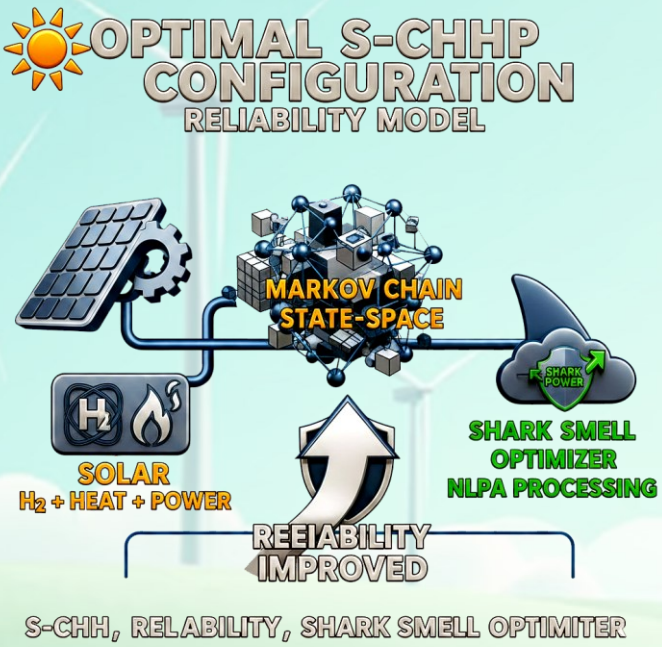

Use your device to scan and read the article online

Citation

M. Pirmohammad, S. Bagheri, R. Ghanizadeh, and M. R. Miveh, "Optimal Configuration of Solar Combined Hydrogen, Heat and Power (S-CHHP) by Considering Reliability Model," *Journal of Green Energy Research and Innovation*, vol. 2, no. 4, pp. 45-57, 2025.

https://doi.org/10.61882/jgeri.2.4.45

Journal of Green Energy Research and Innovation 2.4 (2025) 45-57

Online ISSN: 3041-9018

Journal of Green Energy Research and Innovation

Journal Homepage: www.jgeri.araku.ac.ir

Optimal Configuration of Solar Combined Hydrogen, Heat, and Power (S-CHHP) by Considering Reliability Model

Mojtaba Pirmohammad Talatape [1], Sajad Bagheri [1,*], Reza Ghanizadeh [2], Mohammad Reza Miveh [3]

[1] *Department of Electrical Engineering, Ar.C., Islamic Azad University, Arak, Iran.*

[2] *Department of Electrical Engineering, Ur.C, Islamic Azad University, Urmia, Iran.*

[3] *Department of Electrical Engineering, Tafresh University, Tafresh, Iran.*

A R T I C L E I N F O

Keywords:
S-CHHP,
Markov chain,
Shark Smell Optimizer.

Article History:
Received: 01 July 2025;
Revised: 29 August 2025;
Accepted: 01 December 2025.

Article type:
Research Article

* ***Corresponding author***
E-mail address
Sajad.bagheri@iau.ac.ir (S. Bagheri)

A B S T R A C T

Environmental and economic concerns of utilizing fossil fuels reveal the need to use alternative sources. Due to various kinds of energy demands, choosing the proper generation units is the main aim of energy administrators. Simultaneous generation units are the proper choice to meet several kinds of demands. Combined hydrogen, heat, and power (CHHP) is a cogeneration system to generates three kinds of energy demands. Presenting the comprehensive reliability model of CHHP is the main part of this study. State-space and continuous Markov models with hydrogen, heat, and power generation systems are considered in the reliability model of CHHP. Loss of load expectation (LOLE) and expected energy not supplied (EENS) are considered as reliability indices to verify the efficiency of the proposed reliability model of the CHHP. Due to the important role of communication and data gathering, sending and receiving, the necessity to have a system to minimize the errors in data gathering and processing, and sending is unavoidable. Natural language program (NLP) is the best tool for managing data received, processing, and sending within the system with high accuracy.

1. Introduction

Rising energy demand and inefficiencies in production may soon outstrip supply, forcing the countries to import energy and causing major economic and social problems [1]. Reference [2] examines water-energy systems as a vital component of modern energy policies, analyzing hydraulic efficiency (EH) and annual water output. Findings show that multi-pump stations achieve 97% EH, surpassing mono-pump systems. The research also tackles power management challenges in PV-powered water stations using a Mixed Integer Linear Programming (MILP) model to optimize both solar power use and water production. Additionally, it highlights cogeneration—simultaneous production of multiple energy types—as a solution to boost efficiency, cut primary energy use, and reduce emissions. A key example is Combined Hydrogen, Heat, and Power (CHHP), integrating electrolyzers, fuel cells, and storage for cleaner, more efficient energy systems. In [3], the author presents a smarter way to manage renewable energy and storage, making electricity distribution more cost-effective, reliable, and eco-friendly. Tests and case studies show that this approach works well. By optimizing the solar-hydrogen storage system, the study improves the network's performance, saves money, and reduces environmental impact compared to traditional energy management methods. It also discusses a CHHP system by emphasizing reliability modeling (using state-space and Markov models) and the need for efficient data handling via Natural Language Programming (NLP). Paper [4] presents a reinforcement learning (RL)-based energy management system (EMS) for multi-energy microgrids (MEMGs), optimizing both economic efficiency and system durability. Literature [5] presents a scalable approach to microgrid planning by incorporating dynamic degradation cost models for both solar PV systems and battery storage, addressing the shortcomings of conventional fixed or computationally intensive methods. Choosing and using simultaneous production systems depends a lot on the desired site, rules, and how to use them. Some of the effective factors are as follows:

- Cogeneration system design depends heavily on fuel and electricity prices, as well as thermal energy requirements (temperature/pressure). For instance, high-cycle systems suit a sugar plant (120°C), while cement plants (1450°C) need low-cycle systems, with demand patterns dictating type and size [6-9].
- The hydrogen/heat-to-power ratio, fuel availability, and demand reliability critically influence cogeneration system selection. Matching consumer needs with unit specifications—while balancing cost, redundancy, and grid connectivity—determines whether the system meets partial/full demand or sells excess output [10-14].
- Environmental laws may prohibit the use of some fuels due to high pollution, which may limit the choice of the type of cogeneration system [15].

Optimal sizing and siting of the CHHP in the distribution power system with considering technical and economic functions as provided in [16]. In [17], a new approach to empirical electrical modelling of a fuel cell, an electrolyzer, or a regenerative fuel cell was discussed. Modelling system uncertainties in the planning problem helped to give comprehensive results. In [18], the authors used the Monte Carlo method (MCM) to predict system uncertainties. Improving reliability indices in the planning problem is the main aim of several works of literature. In [19], the authors used a reliability–constrained optimization approach to model participation of private investors and distribution network operators. To enhance the reliability features of the multi-microgrid, the authors suggested a fair electricity market strategy [20]. To improve patterns of energy consumption of the consumers, some programs are introduced as demand responses. These programs are in two cases: time (or price) based and incentive-based programs. Reference [21] presented the impacts of employing a demand response program in the optimal sizing of a CHP unit. Reference [22] introduced a three-stage hybrid robust–stochastic framework for modeling the coordinated operation of CHP units and compressed-heat energy storage, formulated as a MILP problem.

In this paper, solar-based CHHP is proposed to be used as a generation unit. The reliability model of S-CHHP will be introduced and used to meet the residential-based load. Loss of load expectation (LOLE) and expected energy not supplied (EENS) are used as reliability indices. MILP is adopted and modelled in the general algebraic model system (GAMS) software.

The main contribution of this paper is classified as follows:

- Presenting a reliability model of solar-based CHHP (S-CHHP)
- Utilizing long short-term memory (LSTM)-convolutional neural network (CNN) to predict system uncertainties
- Utilizing K-means clustering as a scenario reduction method

The rest of the paper is organized as follows. Section 2 provides the CHHP model. Section 3 presents the main objective function. All of the simulation results are evaluated in Section 4. Section 5 concludes the work.

2. Problem definition

- Definition of S-CHHP features

The CHHP system, comprising an electrolyzer, fuel cell, and thermal/hydrogen storage, effectively meets residential energy demands. Since electrolyzers have low efficiency, photovoltaic (PV) systems directly power them, as illustrated in Figure 1 [23].

- Reliability modelling of the S-CHHP

In this study, the input power of the electrolyzer is fed by a PV system. For the reliability modelling of the S-CHHP, the series of PV, thermal, hydrogen, power, and CHHP are considered as the Figure 2. In the S-CHHP, the reliability of the system is calculated by multiplying the probability of the series subsystem. The number of failures in the year and the frequency of repairs in that year are known as two important reliability parameters: failure time and repair time.

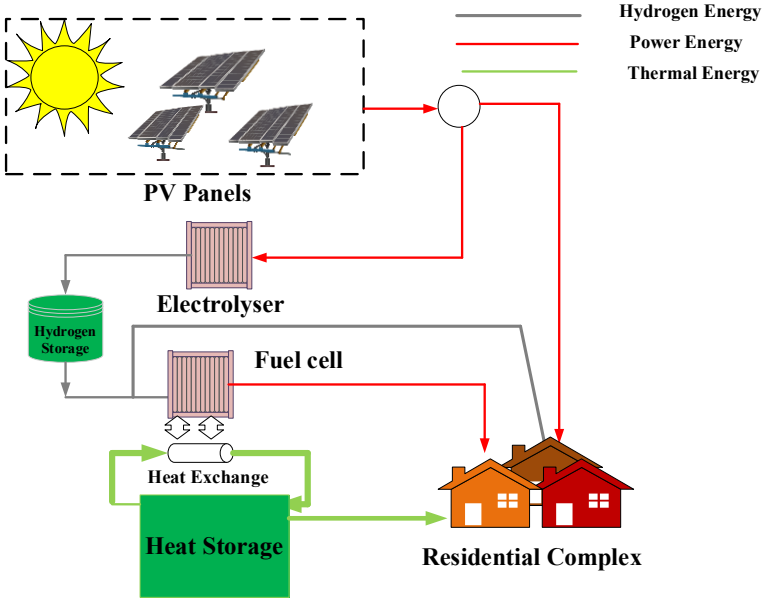

Figure 1. The proposed S-CHHP.

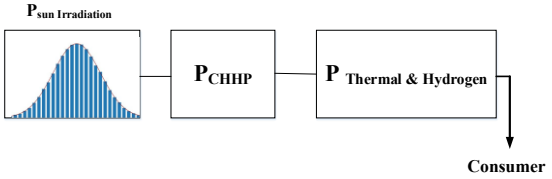

Figure 2. Reliability representation of S-CHHP.

The reliability of S-CHHP is defined as Equation (1).

$$R_{S-CHHP} = R_{PV} \times R_{Th} \times R_{Power} \times R_{Hyd} \tag{1}$$

Figure 3 shows 11 states that can happen in the operational condition of S-CHHP.

- Markov Model

Markov modeling provides an effective reliability analysis for memoryless systems with constant failure/repair rates, where availability becomes more critical than reliability in multistate systems due to computational complexity [24]. Figure 3 shows 11 states that can happen in the operational condition of S-CHHP.

Availability of subsystems is defined as follows:

$\text{Availability}_{\text{Thermal}} = \text{P1} + \text{P2}$ $\text{Availability}_{\text{Power}} = \text{P1} + \text{P5}$ $\text{Availability}_{\text{Hydrogen}} = \text{P1} + \text{P3}$

- Problem Formulation

The main function of this paper is to increase the reliability level of the proposed CHHP-based energy system by reducing total annualized costs and considering system constraints. The proposed planning problem formulation is defined as Equation (2).

$$OF = \min\left(IC^{CHHP} + \sum_{s=1}^{N_s}\sum_{t=1}^{8760} \pi_s \times (IRL_{s,t} + OC_{s,t})\right) \tag{2}$$

IC and *OC* are the investment cost and operational cost, respectively. IRL is the reliability-based cost and is defined as Equation (3).

$$IRL = EENS \times C_{Loss} \quad (\$ / year) \tag{3}$$

The proposed planning problem has been applied to the large residential load with thermal, hydrogen, and power demands.

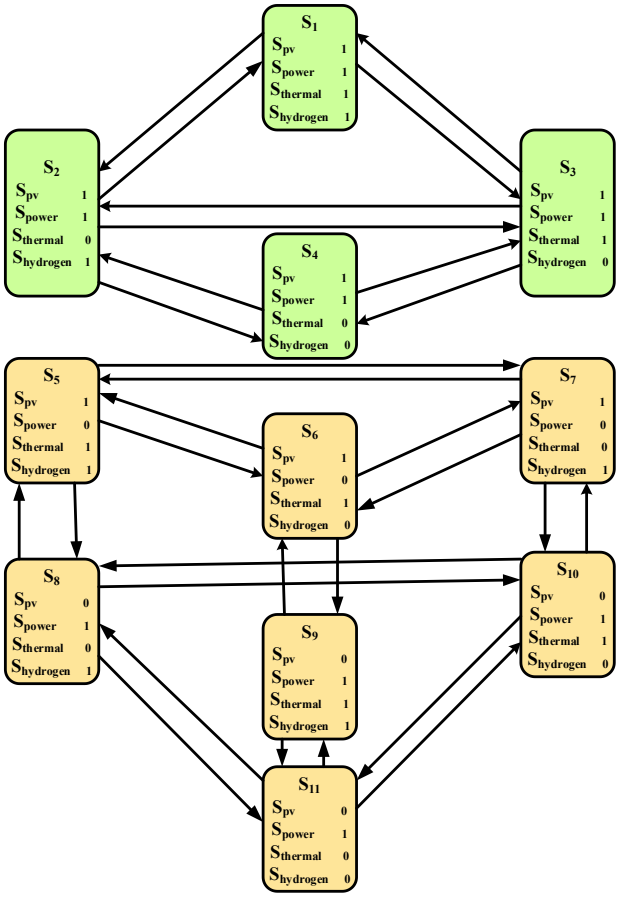

Figure 3. Markov block diagram of S-CHHP.

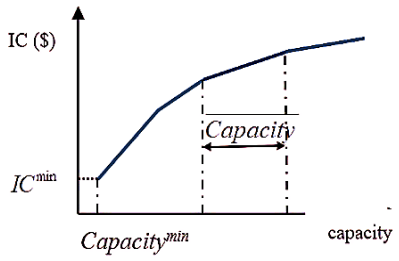

Figure 4. The linear model of investment cost.

2.1. Investment

The increasing size of the generation unit has an inverse relation with the price of its components ($/kW). Figure 4 shows the relation between size and investment cost of components.

The linear form of the (IC-Capacity) curve is defined in Equation (4) [25].

$$IC = IC^{\min} \times \delta_1 + \sum_{k=1} slope_k \times capacity_k \tag{4}$$

$$\delta_k \le 1 + \frac{capacity_{k-1} - capacity_{k-1}}{capacity_{k-1}} \tag{5}$$

δ_k is the binary variable, and $slope_k$ is the slope of the *kth* segment.

2.2. Operational constraints of S-CHHP

This section defines the operational constraints of S-CHHP.

- **PV**

The electrical output of a photovoltaic installation is primarily influenced by ambient temperature, the intrinsic efficiency of the PV modules, and the intensity of the solar irradiance they absorb. These parameters jointly determine the system's real power production, which is formally expressed through Equation (6) [26]. In practical operation, variations in any of these factors—such as temperature-induced efficiency losses or fluctuations in incident sunlight—directly translate into measurable changes in PV performance. This relationship forms the basis for accurate modeling, forecasting, and optimization of PV energy generation under diverse environmental conditions.

$$P_{out,t}^{PV} = \eta^{PV} \times A \times (25 - T_{amb}) \times Ir_t \tag{6}$$

- **Electrolyzer**

Hydrogen and oxygen are separated from water using an electrolyzer, which drives an electric current through two physically isolated electrodes to initiate the decomposition process. The electrolyzer's power output follows the relationship defined in Equation (7) [27]. In operational settings, the electrical input, electrode characteristics, and system efficiency all influence the rate and quality of gas production, making the governing equation essential for performance assessment and system design.

$$P_t^{Out\_EL} = P_t^{Out\_SPL} \times \eta^{EL} \tag{7}$$

- **Fuel cell**

A fuel cell converts the chemical energy stored in hydrogen and oxygen directly into electrical power through an electrochemical reaction rather than combustion. Its electrical output is quantified using the relationship expressed in Equation (8) [28]. In practice, this output depends on factors such as reactant flow rates, cell temperature, and internal losses, making the governing equation a key reference for evaluating performance and integrating the device into broader energy systems.

$$P_t^{FuelCell} = P_t^{HSS\_Fuelcell} \times \eta^{fuelcell} \tag{8}$$

- **Hydrogen storage**

Hydrogen storage serves as a buffering component that stabilizes the operation of intermittent electrolyzers and fuel cells, ensuring a continuous supply of hydrogen regardless of production or consumption fluctuations. The corresponding hydrogen flow rate associated with the storage unit is characterized by the relation given in Equation (9) [29], which governs how hydrogen is charged into or discharged from the storage system under varying operating conditions.

$$HSS_t = HSS_{t-1} + \eta^{PH} \times P_t^{PH} - \frac{P_t^{HP}}{\eta^{HP}} \tag{9}$$

- **Heat storage**

Heat transfer within the thermal storage system is governed by the relation expressed in Equation (10) [30]. This formulation specifies the rate at which heat is accumulated or released by the storage unit, reflecting its dynamic response to charging and discharging conditions in the broader energy system.

$$Heat_t^{HS} = \eta^{HS} \times Heat_{t-1}^{HS} + Heat_{t-1}^{HS-in} - Heat_{t-1}^{HS-out} \tag{10}$$

2.3. Power, heat, and hydrogen balance equation

The governing constraints for maintaining power, heat, and hydrogen balance within the system are specified in Equations (11) through (13). These expressions ensure that all inflows and outflows of energy and mass remain consistent with the operational and physical limits of the integrated system.

$$P_t^{S-CHHP} + P_t^{Grid-Sell} - P_t^{Grid-buy} = P_t^{Load} \tag{11}$$

$$Heat_t^{S-CHHP} = Heat_t^{Storage} + Heat_t^{Load} \tag{12}$$

$$Hyd_t^{S-CHHP} = Hyd_t^{Storage} + Hyd_t^{Load} \tag{13}$$

2.4. Reliability indices

This study employs Loss of Load Expectation (LOLE) and Expected Energy Not Supplied (EENS) as the primary reliability metrics for the system. These indices quantify the likelihood and magnitude of insufficient power supply and are mathematically expressed in Equations (14) and (15), respectively [31]. LOLE measures the expected number of hours in which the system cannot meet the load, while EENS represents the expected energy deficit during these periods, providing a comprehensive assessment of system reliability.

$$LOLE = \sum \pi_s \times \sum_{t=1}^{n\times 8760} LSIX_t \le \overline{LOLE} \tag{14}$$

LSIX is the binary variable equal to 1 when load shading occurs [32].

$$EENS = \sum\sum \pi_s \times \sum_{t=1}^{n\times 8760} LS_t \le \overline{EENS} \tag{15}$$

LS is load curtailment.

3. Optimization Algorithm

3.1. Shark smell optimization (SSO)

The Shark Smell Optimization (SSO) algorithm is a novel population-based optimization technique inspired by sharks' natural ability to detect and move toward prey, representing an optimal solution. In this approach, the initial population is generated by assigning potential positions to each shark, which serve as candidate solutions in the search space.

$[X_1^1. X_1^2. \cdots . X_{NP}^1]. NP =$ Population Size

So, the ith initial location vector, which represents the ith initial option solution for the optimization problem, is given by Equation (16).

$$X_i^1 = [x_{i.1}^1. x_{i.2}^1. \cdots . x_{i.ND}^1]. \qquad i = 1.2. \cdots . N \tag{16}$$

In this formulation, x_{ij} represents the jth dimension of the ith shark's initial position, corresponding to the jth decision variable of the ith individual X_i, with the total number of decision variables denoted as ND. During the optimization process, the sharks update their positions and velocities as they move toward the prey, with the velocity vector of the ith shark defined by Equation (17).

$$V_i^1 = [v_{i.1}^1. v_{i.2}^1. \cdots . v_{i.ND}^1] \tag{17}$$

The movement of the shark towards the prey is based on its "forward smell" motion, and its "rotation" is based on a gradient function, given by Equation (18) [33].

$$V_i^k = \eta_k \cdot R1 \cdot \nabla(OF)|_{X_i^k} \tag{18}$$

For a population size of $i = 1, \ldots, NP$ and iteration index $k = 1, \ldots, k_{\max}$, where $k_{\max}$ denotes the maximum number of algorithmic iterations, the objective function (OF) represents the performance metric to be optimized. The gradient of the objective function, ∇(OF), provides directional information for movement toward optimal solutions. Building upon the previous velocity of the individual shark, the current velocity at iteration k can be expressed as in Equation (19). This formulation enables the algorithm to dynamically adjust the search direction and step size, thereby enhancing convergence efficiency and the ability to explore the solution space effectively in population-based optimization scenarios. Additionally, by incorporating the gradient information, the algorithm achieves a balance between global exploration and local exploitation, which is critical for avoiding premature convergence and ensuring robust optimization performance.

$$\left|V_{i.j}^k\right| = Min\left[\left|\eta_k \cdot R1 \cdot \frac{\partial(OF)}{\partial x_j}\right|_{X_{i.j}^k} + \alpha_k \cdot R2 V_{i.j}^{k-1}\right| . \left|\beta_k V_{i.j}^{k-1}\right|\right] \tag{19}$$

In this formulation, $j = 1, \ldots, ND$, where ND represents the number of decision variables. The parameters $\eta_k \in [0,1]$ and $\alpha_k \in [0,1]$ are user-defined coefficients within the SSO algorithm, governing the relative influence of the newly computed velocity component in comparison to the previous velocity during the k-th iteration. The terms R_1 and R_2 are random variables uniformly sampled from the interval [0, 1], introducing stochasticity to the search process. Additionally, β_k denotes a rate-limiting factor applied in iteration k to control the maximum allowable velocity change, thereby preventing overshooting of the optimum.

Based on these velocity updates, the projected position of each shark, reflecting its forward movement toward the prey, can subsequently be determined as expressed in Equation (20). This step is fundamental in ensuring that the algorithm balances exploration and exploitation, enabling effective navigation through complex, multidimensional solution spaces while maintaining convergence stability.

$$\mathrm{Y}_i^{k+1} = \mathrm{X}_i^k + \mathrm{V}_i^k \Delta t_k \tag{20}$$

So, Δt_k determines the time interval in the kth iteration. Therefore, the rotational movement of the shark can be expressed as Equation (21).

$$Z_i^{k+1.m} = \mathrm{Y}_i^{k+1} + \mathrm{R3} \cdot \mathrm{V}_i^{k+1} \tag{21}$$

In this context, $m = 1, \ldots, M_a$, where $M_a$represents the total number of discrete points along the shark's circular search trajectory during each iteration. The variable $R_3$is a random number uniformly sampled from the interval $[-1, +1]$, introducing variability into the search pattern to enhance exploration. Mdenotes the total number of points evaluated along the circular path in a given iteration. At each of these points, the objective function (OF) value is calculated, and the shark's updated position is determined according to Equation (22). This mechanism allows the algorithm to exploit local regions effectively while simultaneously exploring the surrounding solution space, improving the likelihood of identifying global optima in complex, multidimensional optimization problems.

$$X_i^{k+1} = argmax\left\{OF\left(\mathrm{Y}_i^{k+1}\right) \cdot OF\left(\mathrm{Z}_i^{k+1.1}\right). \cdots . OF\left(\mathrm{Z}_i^{k+1.M}\right)\right\} \tag{22}$$

In this formulation, the operator arg max $\{\cdot\}$ identifies the argument that maximizes the objective function $OF(\cdot)$, effectively selecting the optimal candidate from the evaluated positions. Upon completing the iterative process, each individual in the population updates its position according to the described operators, and the overall best-performing individual is reported as the solution at the final iteration of the algorithm. Figure 5 illustrates the modeled behavior of a shark navigating toward an odor source, guided by the gradient of concentration, which serves as an analogy for the algorithm's directed search towards the global optimum.

The New SSO (NSSO) introduces an additional operator in its first step to enhance the search process by considering the shark's best position in relation to its neighborhood. This is achieved by evaluating the neighborhood using best-neighbor information. Specifically, the algorithm calculates the Euclidean distance between the position of shark $X_i^1$and all other candidate solutions. These individual distances, denoted as $d(i,j)$, are then averaged to obtain the mean distance mdi, which quantifies the spatial distribution of the neighborhood. This metric allows the algorithm to guide the shark more effectively toward promising regions in the search space, leveraging local information for improved convergence.

$$md_i = \frac{\sum_{j=1}^{M} d(i.j)}{M-1} M \tag{23}$$

In this framework, a candidate solution x_j is considered part of the neighborhood of X_i^1 if its distance $d(i,j)$ is smaller than the mean distance mdi, ensuring that only sufficiently close solutions influence the shark's movement.

To address premature convergence, the second step incorporates an abandonment mechanism. Here, a parameter $l(i)$is introduced for each shark $(i = 1, \ldots, M)$ and initially set to zero. If a shark's position does not improve during an iteration, the parameter is incremented as $l(i) = l(i) + 1$; otherwise, it is reset to zero. When the stagnation persists beyond a threshold, the parameter reaches a maximum value L, signaling the need for exploration. This mechanism allows the algorithm to adaptively modify the search behavior, encouraging movement toward new regions in the solution space and is formalized in Equation (24).

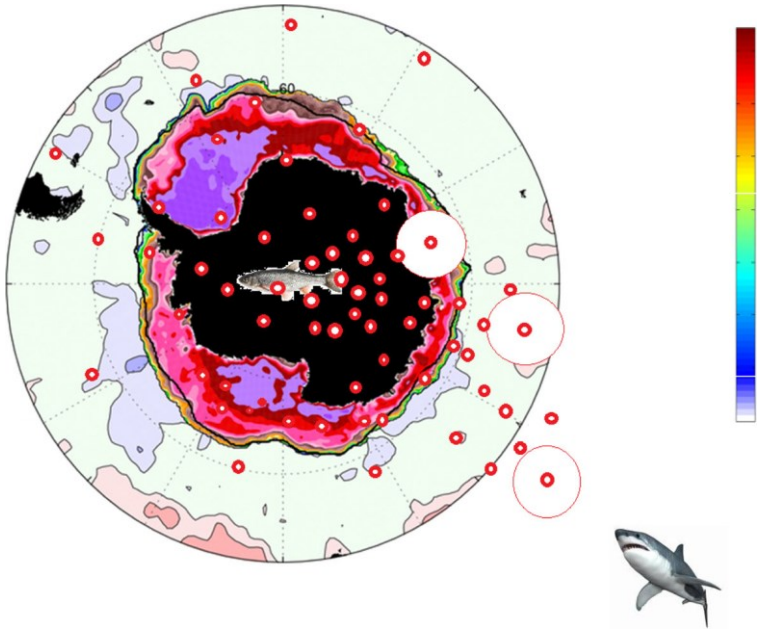

Figure 5. Shark smell behavior.

$$x_{new} = \tau^{*} Pg + \emptyset^{*}(Pg - x_i) \quad (24)$$

In this formulation, $\emptyset$ represents a randomly generated number within the range [-1, 1], while τacts as a weighting factor that regulates the influence of the global best solution during the current iteration, increasing progressively over time. Using this equation, the new position $x_{\text{new}}$is determined with considerable randomness, allowing the search to explore broadly initially and then focus closely around the global best solution $P_g$in the final stages. For the final refinement step in the algorithm, three random variables from the SSO framework—R_1 and R_2associated with forward movement, and R_3related to rotational movement—are generated according to Equations (25) and (26), enhancing the stochastic exploration and exploitation balance.

$$C_{k+1} = 4C_k(1 - C_k) \quad for\ R1\ and\ R2 \quad (25)$$

$$C'_{k+1} = 2C_{k+1} - 1 \quad for\ R3 \quad (26)$$

In this approach, $C_k$and $C_{k+1}$are values produced by the chaotic pendulum operator, with $C_k, C_{k+1} \in (0,1)$and $C'_{k+1} \in (-1,1)$. The operator is initialized by generating C_0randomly within the interval (0,1), ensuring that $C_0 \notin \{0.25, 0.5, 0.75\}$to avoid fixed points that could reduce chaotic behavior. Additionally, a random mutation operator is applied to each $G^g_{i,j}$with a predefined probability p_b. This mutation enhances population diversity, preventing premature convergence and improving the algorithm's exploratory capability, as described in Equations (27) and (28).

$$G^g_{\text{i.j}} = rand(L\,B_j . U\,B_j). \quad if\ \ rand\ (0.1) < pb \quad (27)$$

$$G^g_{\text{i.j}} = G^g_{\text{i.j}} \quad otherwise \quad (28)$$

A. Long-Short term memory (LSTM)

In recent years, LSTM neural networks have gained significant attention due to their ability to address long-term dependencies in sequential data [34]. LSTM networks are specifically designed to retain information over extended periods, making them highly effective at learning temporally separated patterns. Like all recurrent neural networks (RNNs), LSTMs consist of a chain of interconnected modules; however, unlike simple RNNs with basic recurrent units, LSTM modules have a more sophisticated internal architecture.

A fundamental component of LSTM networks is the cell state C_t, which acts as a memory pathway capable of selectively adding or removing information. This functionality is regulated by specialized structures known as gates, which determine how information flows into, through, and out of the cell. At each time step t, the input $X_t$is processed by the input gate I_t, which controls the amount of new information stored in the cell state C_t. Simultaneously, the forget gate $F_t$regulates the retention of the previous cell state C_{t-1}, selectively discarding irrelevant information. Finally, the output gate determines which portion of the updated cell state contributes to the network's output h_t. The dynamics of these gates and the updated cell state are mathematically defined in Equations (29)–(31), capturing the flow and transformation of information within the LSTM unit.

$$C_t = F_t \times C_{t-1} + I_t \times (tanh(W_c \times [O_{t-1}. X_t] + b_c)) \quad (29)$$

$$I_t = \sigma(W_i \times [O_{t-1}.X_t] + b_i) \quad (30)$$

$$F_t = \sigma(W_f \times [O_{t-1}. X_t] + b_f) \quad (31)$$

In the preceding equations, W_c, W_f, and $W_i$represent the weight matrices associated with the cell, forget, and input gates, respectively. The term O_{t-1}denotes the output of the LSTM cell from the previous time step, while $X_t$corresponds to the current input at time t. The vectors b_c, b_i, and $b_f$are the bias terms applied to the cell, input, and forget gates, facilitating the adjustment of the gate activations during network training. In this case, the output is as Equation (32).

$$O_t = \sigma_t \times tanh\,(C_t) \quad (32)$$

3.2. Convolutional Neural Network (CNN)

CNNs utilize multilayer perceptrons with adaptive weights to learn nonlinear input-output relationships through convolutional layers (feature extraction), pooling (dimensionality reduction), and fully connected layers (final feature integration), where 3D filters in the initial layer generate output feature maps. To obtain the mapping relation of the first layer from the one-dimensional input $x = (x_t)\_(t=0)\hat{}(N-1)$ with size N, the filter combinations w^1_h for $h = 1,\ldots,$ and M_1 are as Equation (33).

$$a^1(i.h) = (w^1_h * x)(i) = \sum_{j=-\infty}^{\infty} w^1_h(j)x(i-j) \quad (33)$$

In this equation w^1_h and a^1 belong to the sets $R^{1\times k\times 1}$ and $R^{1\times N-k+1\times M_1}$, respectively.

Similar to feedforward neural networks, the output is processed through a nonlinear activation function $h$to yield $f = h(a)$. For each subsequent layer $l = 2, \ldots, L$in the mapping network, the feature map $f^{(l-1)} \in \mathbb{R}^{1\times N_{l-1}\times M_{l-1}}$, with dimensions $1 \times N_{l-1} \times M_{l-1}$, is combined with the output from the preceding convolution filter. This operation produces the mapped feature map $a^l \in \mathbb{R}^{l\times N_l\times M_l}$, as expressed in Equation (34).

$$a^l(i.h) = (w^l_h * f^{l-1})(i) = \sum_{j=-\infty}^{\infty}\sum_{m=1}^{M_{l-1}} w^l_h(j.m)f^{l-1}(i-j.m) \quad (34)$$

3.3. Combinational LSTM and CNN (CNN-LSTM)

This section presents our hybrid model for short-term load forecasting (STLF). The overall architecture of the CNN-LSTM-based deep learning network applied to Urmia city is illustrated in Figure 6. The CNN feature extraction module consists of three one-dimensional convolutional layers, each followed by Max-Pooling (to reduce spatial dimensions) and ReLU activation functions (to maintain gradient stability). Early convolutional layers focus on capturing low-level features, while the pooling layers reduce positional variance and computational load.

K-means clustering

K-Means is an iterative clustering algorithm that partitions unlabeled data into 'k' distinct, non-overlapping groups by minimizing within-cluster variances (using squared Euclidean distances) while maximizing between-cluster separation, following the Expectation-Maximization approach with 'k' requiring predefinition.

Step 1: Determine the number of clusters by selecting the value of K.

Step 2: Initialize K centroids, either randomly or through a specific calculation. The Euclidean distance is used to select the initial centers.

Step 3: Assign each data point to the nearest centroid, forming K initial clusters.

Step 4: Compute the mean of each cluster and update the centroid to this new value.

Step 5: Reassign all data points to the nearest updated centroid, refining the cluster assignments.

Step 6: Repeat the centroid update and reassignment steps until no significant changes occur, indicating convergence.

Step 7: Finalize the clustering model, which is now ready for use.

Equation (35) is the objective function of the k-means clustering algorithm. It measures how “tight” the clusters are. Lower J means better, more compact clusters.

$$J = \sum_{k=1}^{k} \sum_{p_i \in s_k} (p_i - c_k)^2 \tag{35}$$

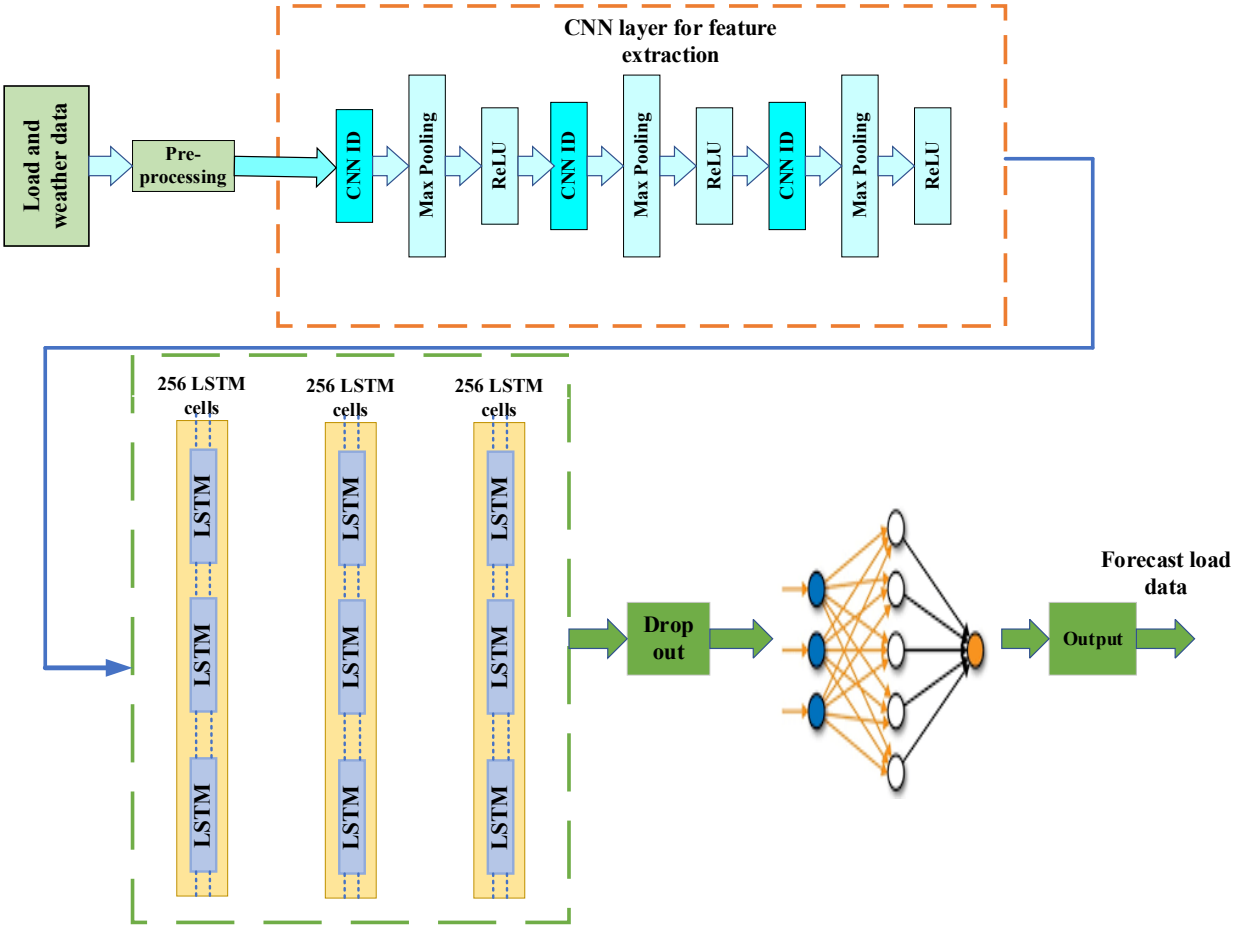

Figure 6. LSTM model.

4. Simulation results

In this section, we will examine the performance of the methods presented in the article and compare them with the proposed methods of past research to identify their strengths and weaknesses. Also, the criteria of good or bad performance of these methods will be introduced, and by using practical simulations with real data, load prediction charts and tables will be presented.

4.1. 4.1. Input data

Figure 6 illustrates the typical demand for electricity, heat, and hydrogen in a day. The electric, heat, and hydrogen base loads are 1800, 3500, and 1000kW, respectively. Table 1 gives the parameters of S-CHHP. Table 2 tabulates the time of use-based demand response and fuel cell parameters.

4.2. The optimal size of CHHP

The rest of the scenarios after employing the k-means clustering algorithm are given in Table 3. Figures 7-11 show the predicted values by LSTM. The lowest MAPE error values can be achieved using the deep learning scheme proposed by CNN-LSTM in this thesis. The closest MAPE value to our proposed method is the GRU network in the reference, which is obtained by a powerful STLF tool. Compared to the reference results, MAPE improvement is achieved at least 0.2%, which can lead to extensive cost savings in electric power generation plants. Root Mean Square Error (RMSE) and Mean Absolute Percentage Error (MAPE) have been used to evaluate the accuracy of the proposed model. RMSE measures the amount of error between two data sets according to Equation (36).

$$RMSE = \sqrt{\frac{1}{n}\sum_{i=1}^{n}\left(\hat{Y}_i - Y_i\right)^2} \tag{36}$$

Here, $Y_i$represents the observed load at time i, while $\hat{Y}_i$denotes the forecasted value. The MAPE is used as a metric to evaluate the accuracy of a prediction model. It expresses the forecast error as a percentage and is computed according to Equation (37).

$$MAPE = \frac{1}{n}\sum_{i=1}^{n}\left|\frac{\hat{Y}_i - Y_i}{Y_i}\right| \tag{37}$$

Table 4 presents a comparative analysis between the proposed STLF model and existing forecasting models reported in the literature.

Table 1. CHHP parameters.

Unit	CHHP			PV						
Parameter	$\eta^{Electrolyser}$	η^{HE}	ω	η^{PV}	S	T_a	If	Ir	(year) τ	α
Value	0.7	0.92	0.75	15.5%	750	25	9%	9%	15	2%

Table 2. Demand response parameter.

TOU Program			Fuel Cell
Peak	Normal	Low	
20–23	7:00–19:59	0:00–6:59	$\eta^{Fuel\ cell}$
0.48($/kWh)	0.35($/kWh)	0.22($/kWh)	0.75

Table 3. Scenarios after employing scenario reduction.

Scenario	1	2	3	4	5
Probability	0.012	0.043	0.387	0.023	0.068
Scenario	6	7	8	9	10
Probability	0.033	0.017	0.117	0.2	0.1

Table 4. Results of different prediction methods.

Forecasting Method	MAPE
DNN	1.32
RNN	1.19
LSTM	1.01
GRU	0.84
The Proposed CNN-LSTM	0.61

Obviously, the lowest MAPE error values can be achieved using the CNN-LSTM deep learning scheme proposed in this thesis. The closest MAPE value to our proposed method is the GRU network in the reference, which is obtained by a powerful STLF tool. Compared to the reference results, MAPE improvement is achieved at least 0.2%, which can lead to extensive cost savings in electric power generation plants. The storage efficiency is 90%, its minimum and maximum energy values are 100 and 260 kWh, respectively, and finally, its initial and final energy values are considered to be 180 kilowatt hours. The results of the optimal planning problem are given in Table 5. The value of the lost load is 10 $/kWh, the cost of providing the reservation is 0.4 cents/kWh, and the duration of the reservation is assumed to be 1 hour. Daily costs of planning problem are illustrated in Figure 12. Loss of load probability (LOLP) in the 24 hours is shown in Figure 13.

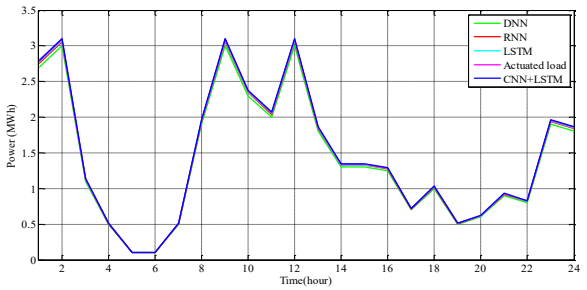

Figure 7. Demand prediction (MW).

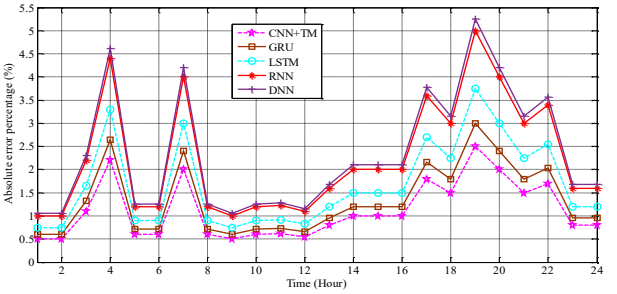

Figure 8. Electrical load.

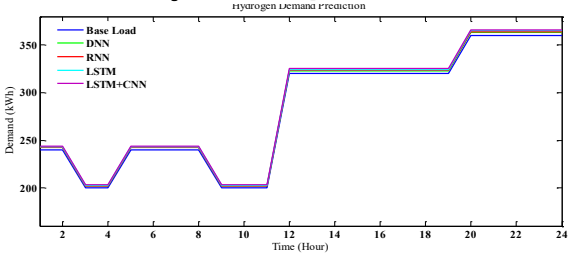

Figure 9. Hydrogen demand.

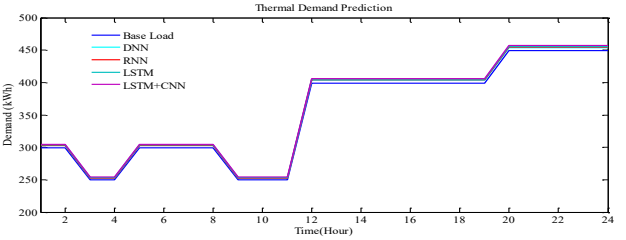

Figure 10. Heat demand.

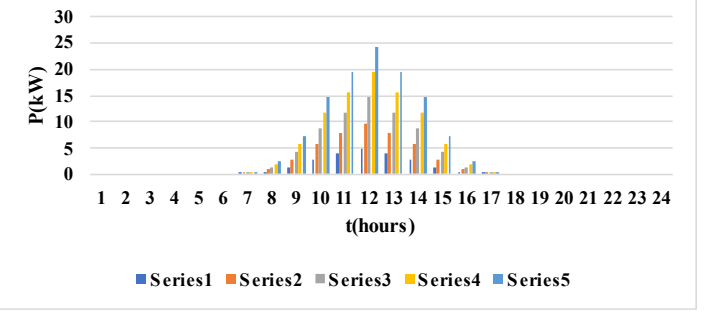

Figure 11. Solar irradiation.

Table 5. Optimal planning solutions.

		Without a heat & hydrogen tank	With a heat & hydrogen tank
Total net present cost ($*10^6)		8.1564	7.8295
Operation cost ($)		3511433 $\pm$ 25408	3599251 $\pm$ 25426
Payback period (year)		6.3	5.4
IRR (%)		28	30
CHHP capacity (KW)	Unit 1	1100	1180
	Unit 2	1082	1095
PV capacity (kW)	Unit 1	400	420
	Unit 2	280	0
LOLE (days/10yrs)	Electrical	0.92	0.94
	Thermal	0.84	0.90
	Hydrogen	0.80	0.82
EENS (kWh/year)	Electrical	600	580
	Thermal	1320	2400
	Hydrogen	860	920

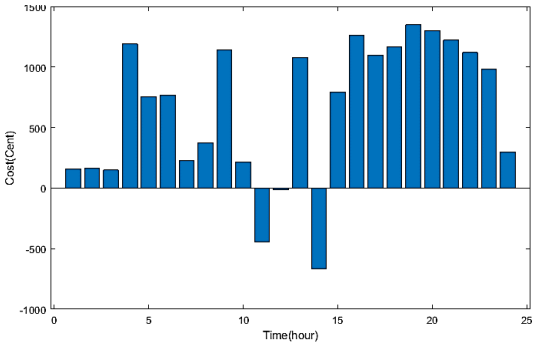

Figure 12. Daily total costs of S-CHHP.

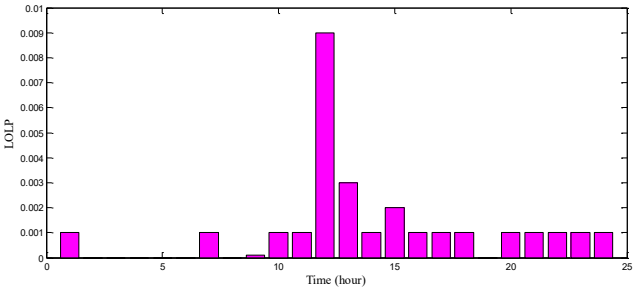

Figure 13. LOLP index.

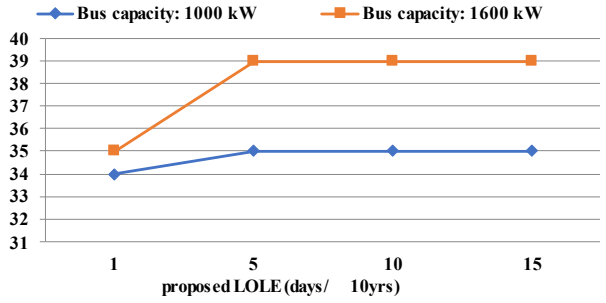

Figure 14. IRR of the proposed problem.

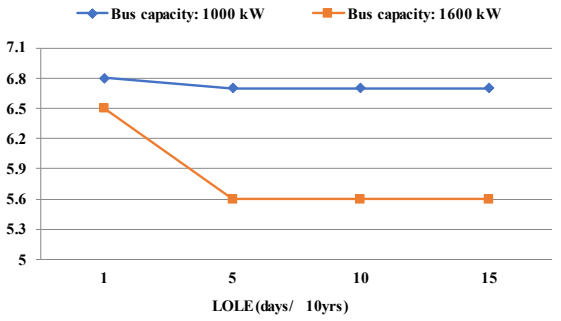

Figure 15. Payback duration in the planning horizon.

4.3. Economic parameter

In this section, the sensitivity of the internal rate of return (IRR) and payback duration i*n* the planning horizon and with the proposed LOLE value are analyzed. Figure 14 shows the IRR values in two allowed exchangeable power with the upstream grid. Figure 15 shows the payback duration changes in the planning horizon. As it is clearly seen from this figure, the payback duration time is reduced by increasing power exchange between the upstream network and the proposed CHHP. Furthermore, considering grid grid-connected bus, the value of IRR for the presented paper is increased. LSTM is used to model system uncertainties.

5. Conclusion

The S-CHHP represents an innovative cogeneration system designed to simultaneously generate hydrogen, thermal energy, and electrical power. This study investigates the optimal configuration of the S-CHHP system by formulating a Markov chain model. Reliability and economic performance are assessed using the LOLP and payback period, respectively, while the accuracy of the proposed model is evaluated via RMSE and MAPE metrics. The optimization problem is addressed using the SSO algorithm. Comparative analysis with alternative prediction approaches demonstrates the effectiveness and superior performance of the proposed method.

References

[1] A. Jafari, H. G. Ganjehlou, T. Khalili, and A. Bidram, "A Fair Electricity Market Strategy for Energy Management and Reliability Enhancement of Islanded Multi-Microgrids," *Applied Energy*, vol. 270, 115170, 2020.
[2] M. Abidi, A. B. Rhouma, and J. Belhadj, "Optimal Coordinated Planning of Water-Energy System-Based MILP Algorithm of a Multi-Pump PV Water Station by Deeming Power Commitment," *Electric Power Systems Research*, vol. 220, 109343, 2023.
[3] E. Akbari," Stochastic Scheduling of Integrated System of Solar Resources and Hydrogen Storage in the Smart Distribution Network Considering a Multi-Objective Energy Management Model," Journal of Green Energy Research and Innovation, vol. 2, no. 3, pp. 44-53, 2025.
[4] E. Hosseini, P. García-Triviño, et al., "A Novel Reinforcement Learning-Based Multi-Objective Energy Management System for Multi-Energy Microgrids Integrating Electrical, Hydrogen, and Thermal Elements," *Electric Power Systems Research*, vol. 242, 111474, 2025.
[5] H. Z. Butt, and X. Li, "Enhancing Optimal Microgrid Planning with Adaptive BESS Degradation Costs and PV Asset Management: an Iterative Post-Optimization Correction Framework," *Electric Power Systems Research*, vol. 247, 111785, 2025.
[6] A. Mansoori, M. Parsa Moghaddam, and H. Delkhosh, "A Hybrid Stochastic-Robust Approach for Power System Security-Constrained Scheduling in the Presence of Flexibility Facilities," *IEEE Transactions on Power Systems*, vol. 39, no. 2, pp. 4064–4076, 2024.
[7] M. Omri, M. Jooshaki, A. Abbaspour, and M. Fotuhi-Firuzabad, "Modeling Microgrids for Analytical Distribution System Reliability Evaluation," *IEEE Transactions on Power Systems*, vol. 39, no. 5, pp. 6319–6331, 2024.
[8] Y. Kabiri-Renani, A. Arjomandi-Nezhad, M. Fotuhi-Firuzabad, and M. Shahidehpour, "Transactive-Based Day-Ahead Electric Vehicles Charging Scheduling," *IEEE Transactions on Transportation Electrification*, vol. 10, no. 4, pp. 8235–8245, 2024.
[9] N. Pourghaderi, M. Fotuhi-Firuzabad, M. Moeini-Aghtaie, M. Kabirifar, and P. Dehghanian, "A Local Flexibility Market Framework for Exploiting DERs' Flexibility Capabilities by a Technical Virtual Power Plant," *IET Renewable Power Generation*, vol. 17, no. 3, pp. 681–695, 2022.
[10] H. Ghasemi, E. Shahrabi Farahani, et al., "Equipment Failure Rate in Electric Power Distribution Networks: An Overview of Concepts, Estimation, and Modeling Methods," *Engineering Failure Analysis*, vol. 145, 107034, 2023.
[11] F. K. Alabbas, M. Khalilifar, S. M. Shahrtash, and D. A. Khaburi, "A novel data driven model for voltage stability status prediction and instability mitigation," *International Transactions on Electrical Energy Systems*, vol. 2025, no. 1, p. 6575682, 2025.
[12] M. Taheri, M. Abedini, and F. Aminifar, "A Novel Centralized Load Shedding Approach to Assess Short-Term Voltage Stability: A Model-Free Using Time Series

Forecasting," *IEEE Transactions on Power Delivery*, vol. 38, no. 5, pp. 3076–3083, 2023.
[13] S. Solat, F. Aminifar, A. Safdarian, and H. Shayanfar, "An Expansion Planning Model for Strategic Visioning of Active Distribution Network in the Presence of Local Electricity Market," *IET Generation, Transmission & Distribution*, vol. 17, no. 24, pp. 5410–5429, 2023.
[14] M. A. A. Al-Ja'afreh, G. Mokryani, and B. Amjad, "An Enhanced CNN-LSTM Based Multi-Stage Framework for PV and Load Short-Term Forecasting: DSO Scenarios," *Energy Reports*, vol. 10, pp. 1387–1408, 2023.
[15] J. A. Marquez, M. A. A. Al-Ja'Afreh, et al., "Optimal Planning and Operation of Distribution Systems Using Network Reconfiguration and Flexibility Services," *Energy Reports*, vol. 9, pp. 3910–3919, 2023.
[16] M. H. Shariatkhah, M. R. Haghifam, and M. A. Paqaleh, "Simultaneous Placement of DGs and Capacitors in Distribution Networks—Determining the Optimum Configuration," *Energy Engineering and Management*, vol. 1, no. 1, pp. 11–18, 2023.
[17] R. Khalilzadeh, and M. R. Haghifam, "Planning and Comparing a Pure AC or a Hybrid AC/DC Distribution Network: A Case Study for an Urban Zone and an Industrial Park," *Journal of Iranian Association of Electrical and Electronics Engineers*, vol. 20, no. 2, pp. 77–86, 2023.
[18] M.-A. Efstratiadi, S. Tsakanikas, P. Papadopoulos, and D. R. Salinas, "A Novel Holistic Energy Management System Incorporating PV Generation and Battery Storage for Commercial Customers," *IEEE Transactions on Sustainable Energy*, vol. 15, no. 3, pp. 1475–1485, 2024.
[19] A. Ntafalias, S. Tsakanikas, et al., "Design and Implementation of an Interoperable Architecture for Integrating Building Legacy Systems into Scalable Energy Management Systems," *Smart Cities*, vol. 5, no. 4, pp. 1421–1440, 2022.
[20] Y. Zhou, J. Wu, and W. Gan, "P2P Energy Trading Via Public Power Networks: Practical Challenges, Emerging Solutions, and the Way Forward," *Frontiers in Energy*, vol. 17, no. 2, pp. 189–197, 2023.
[21] R. Bo, L. Bai, et al., "Special Section on Local and Distributed Electricity Markets," *IEEE Transactions on Smart Grid*, vol. 14, no. 2, pp. 1347–1352, 2023.
[22] L. Zhang, J. Li, et al., "High Spatial Granularity Residential Heating Load Forecast Based on Dendrite Net Model," *Energy*, vol. 269, 126787, 2023.
[23] Y. Cai, X. Xu, J. Liu, X. Yu, and H. Jia, "Coordinative Control of Hydropower Plant and Industrial Thermostatically Controlled Loads for Frequency Response," *2023 IEEE Power & Energy Society General Meeting (PESGM)*, pp. 1–5, 2023.
[24] V. Bafandegan Emroozi, and M. Doostparast, "Markov Chain-Based Model for IoT-Driven Maintenance Planning with Human Error and Spare Part Considerations," *Reliability Engineering & System Safety*, vol. 261, 111052, 2025.
[25] R. Rostami, and H. Hosseinnia, "Energy Management of Reconfigurable Distribution System in Present of Wind Turbine by Considering Several Kinds of Demands," *7th Iran Wind Energy Conference (IWEC2021)*, pp. 1–4, 2021.
[26] M. Hemmati, N. Amjady, and M. Ehsan, "Islanded Micro-Grid Modeling and Optimization of its Operation Considering Cost of Energy not Served by an Enhanced Differential Search Algorithm," *Energy Engineering and Management*, vol. 3, no. 4, pp. 2–13, 2023.
[27] S. Rezaeeian, N. Bayat, A. Rabiee, S. Nikkhah, and A. Soroudi, "Optimal Scheduling of Reconfigurable Microgrids in Both Grid-Connected and Isolated Modes Considering the Uncertainty of DERs," *Energies*, vol. 15, no. 15, 5369, 2022.
[28] S. Toghranegar, A. Rabiee, and A. Soroudi, "Enhancing the Unbalanced Distribution Network's Hosting Capacity for DERs Via Optimal Load Re-Phasing," *Sustainable Cities and Society*, vol. 87, 104243, 2022.
[29] M. Zamudio López, H. Zareipour, and M. Quashie, "Forecasting the Occurrence of Electricity Price Spikes: A Statistical-Economic Investigation Study," *Forecasting*, vol. 6, no. 1, pp. 115–137, 2024.
[30] N. Daryani, K. Zare, S. Tohidi, J. M. Guerrero, and N. Bazmohammadi, "Optimal Construction of Microgrids in a Radial Distribution System Considering System Reliability Via Proposing Dominated Group Search Optimization Algorithm," *Sustainable Energy Technologies and Assessments*, vol. 63, 103622, 2024.
[31] Y. Zou, and M. Čepin, "Loss of Load Probability for Power Systems Based on Renewable Sources," *Reliability Engineering & System Safety*, vol. 247, 110136, 2024.
[32] N. Popli, E. Davoodi, F. Capitanescu, and L. Wehenkel, "Machine Learning Based Binding Contingency Pre-Selection for AC-PSCOPF Calculations," *IEEE Transactions on Power Systems*, vol. 39, no. 2, pp. 4751–4754, 2024.
[33] Y. Xie, S. Wang, et al., "Optimized Multi-Hidden Layer Long Short-Term Memory Modeling and Suboptimal Fading Extended Kalman Filtering Strategies for the Synthetic State of Charge Estimation of Lithium-Ion Batteries," *Applied Energy*, vol. 336, 120866, 2023.
[34] D. Pagnani, Ł. Kocewiak, J. Hjerrild, F. Blaabjerg, and C. L. Bak, "Integrating Black Start Capabilities into Offshore Wind Farms by Grid-forming Batteries," *IET Renewable Power Generation*, vol. 17, no. 14, pp. 3523–3535, 2023.

Declaration of competing interest

The authors declare that they have no known competing financial interests or personal relationships that could have appeared to influence the work reported in this paper. The ethical issues, including plagiarism, informed consent, misconduct, data fabrication and/or falsification, double publication and/or submission, redundancy, have been completely observed by the authors.

Bibliography

Mojtaba Pirmohammad Talatape was born in Iran, in 1992. He is currently a PhD student at Islamic Azad University, Arak Branch. He is currently a lecturer at Azad University and manager of the charging department in a private company. He works as the manager of the charging unit in the field of car batteries, UPS and reverse charging, and since 2022, he has been working as a referee for international conferences in the field of electricity distribution and renewable energy. His research interests are power system stability, reactive power control in transmission and distribution systems, power quality studies and electric energy production in renewable systems and related issues.
Email: Pirmomojtaba1372@gmail.com
ORCID: 0000-0002-4587-1403
Contribution Statement: Conceptualization, Data curation, Investigation, Software, Validation, Roles/Writing - original draft, Writing-review & editing.

Sajad Bagheri was born in Arak, Iran, in 1989. He received the Ph.D. degree in electrical engineering from Semnan University, Semnan, Iran, in 2017. He is currently an Assistant Professor with the Electrical Engineering Faculty, Islamic Azad University, Arak Branch, Arak, Iran. Also, he is research Consultant of the Markazi province electric distribution company. His research interests include power system protection, Diagnosis, condition monitoring and detection of winding movement of power transformers and Renewable Resources. Dr. Bagheri is a member of the Young Researchers and Elite Club, the Iranian Wind Energy Association and the Iranian Society of Smart Grid. Also, He was selected as the top Researcher at the universities of Markazi province in the field of electrical engineering and top Researcher of Young researchers and Elite Club of Islamic Azad University, Arak Branch at 2016 & 2019.
Email: Sajad.bagheri@iau.ac.ir
ORCID: 0000-0002-3553-5510
Contribution Statement: Conceptualization, Formal analysis, Investigation, Methodology, Supervision, Validation, Writing-review & editing.

Reza Ghanizadeh was born in Mianeh, Iran, in 1987. He received his B.Sc. degree in Electrical Engineering from University of Mohaghegh Ardabili, Ardabil, Iran, in 2008, and his M.Sc. degree from University of Birjand, Birjand, Iran, in 2012. He is currently working as an assistant professor at Urmia Azad University. His research interests are power system stability, reactive power control in transmission & distribution systems, power quality studies and FACTS devices.
Email: reza.ghanizadeh@iau.ac.ir
ORCID: 0000-0003-2093-0267
Contribution Statement: Visualization, Writing-review & editing.

Mohammad Reza Miveh received his Ph.D. degree in Electrical Engineering from Universiti Teknologi Malaysia (UTM), Malaysia, in 2017. Currently, he is an Assistant Professor with the Department of Electrical Engineering, Tafresh University, Iran. His main research interests include control and protection of large-scale hybrid AC/DC grids, distributed generation and microgrids.
Email: miveh@tafreshu.ac.ir
ORCID: 0000-0002-6130-6703
Contribution Statement: Investigation, Methodology, Resources.